The construction of $Cd_xZn_{1-x}S$-based photocatalysts for enhanced hydrogen generation

K. Y. Li [a,†], Y. Zhou[b,†], H. Y. Wang[c], L. K. Zhou[a], S. P. Zhang[a,*], Y. Lian[b]
[a]*College of Advanced Materials Engineering, Jiaxing Nanhu University, Jiaxing 314001, China*
[b]*College of Material and Textile Engineering, Jiaxing University, Jiaxing 314001, China*
[c]*Jiaxing Eco-Environmental Monitoring Center of Zhejiang, Jiaxing 314001, China*

$Cd_xZn_{1-x}S$ (x=0~1) solid solution photocatalyst with different morphologies was synthesized by solvothermal method using ethylenediamine as solvent. The light absorption of the photocatalyst was varied by changing the morphology and electronic band structure to allow strong visible light response for hydrogen generation. The results showed that the optimum sample $Cd_{0.5}Zn_{0.5}S$ showed a high hydrogen production rate of 2531.3 $\mu mol \cdot g^{-1} \cdot h^{-1}$ with lactic acid as sacrificial agent. Loading with NiS by solvothermal method further improves the hydrogen production performance. The photocatalytic hydrogen evolution rate of $NiS/Cd_{0.5}Zn_{0.5}S$ is 4547.5 $\mu mol \cdot g^{-1} \cdot h^{-1}$, which is 1.80 times that of pure $Cd_{0.5}Zn_{0.5}S$. The mechanism of hydrogen production by $NiS/Cd_{0.5}Zn_{0.5}S$ is also discussed.

(Received September 20, 2023; Accepted November 24, 2023)

Keywords: Energy band regulation, NiS; $Cd_{0.5}Zn_{0.5}S$, Photocatalytic hydrogen production

1. Introduction

Due to the rapid consumption of fossil energy and the resulting serious environmental pollution, the need for the development of clean energy becomes more and more urgent. Hydrogen is considered to be one of the most ideal clean energy because of its high energy density and non-polluting gas emissions after consumption [1]. Among the various hydrogen production technologies, the use of solar energy to drive water splitting to produce hydrogen from semiconductor photocatalysts is a friendly and economical method. Therefore, the development of highly efficient and stable semiconductor photocatalysts is very important for the practical application of photocatalytic hydrogen production [2]. Different types of photocatalysts have been developed, such as metal oxides, metal sulfides, organic polymers, metal-organic frameworks and covalent organic frameworks, et al. However, traditional photocatalytic systems are largely dependent on the band configuration and surface structure of the catalyst, and their performance is still far from satisfactory due to slow electron-hole pair separation efficiency and limited active sites of their surface.

Transition metal sulfides are an important class of semiconductor photocatalysts with narrow band gap and high visible light absorption, which are conducive to catalyzing a series of meaningful redox reactions under mild conditions. Among them, $Cd_xZn_{1-x}S$ has a more negative conduction band bottom potential than CdS, and a narrower band gap than ZnS, so it has a higher visible light absorption capacity and reduction ability to produce hydrogen from water decomposition [3]. Meanwhile, its unique solid solution property can achieve controllable adjustment of the energy band structure by regulating the metal ratio of Zn^{2+} and Cd^{2+} [4-6]. It is of great significance for developing high performance photocatalytic hydrogen production system. However, the original $Cd_xZn_{1-x}S$ still has some defects, such as low photogenerated charge separation and transport efficiency, slow surface reaction kinetics and severe photocorrosion,

* Corresponding authors: 206002@jxnhu.edu.cn
† These authors contributed equally to this work
https://doi.org/10.15251/DJNB.2023.184.1461

which limit its further practical application. In order to improve the catalytic activity of $Cd_xZn_{1-x}S$, the strategies of morphology regulation, element doping, defect regulation and heterojunction structure construction have been widely studied. Metal sulfides are a class of important semiconductor photocatalysts that have been widely studied.

In this work, a series of $Cd_xZn_{1-x}S$ photocatalysts were prepared by solvothermal method using thioacetamide as sulfur source and ethylenediamine as solvent. The band gap of $Cd_xZn_{1-x}S$ was adjusted by changing the molar ratio of Cd/Zn to improve its absorption to visible light. The results show that the optimized $Cd_{0.5}Zn_{0.5}S$ with one-dimensional (1D) nanostructure can effectively promote the transfer and separation of photogenerated carriers under visible light irradiation, and have the best photocatalytic hydrogen production performance. Furthermore, $NiS/Cd_{0.5}Zn_{0.5}S$ nanocomposite was prepared to realize higher photocatalytic performance. A series of characterizations were use to analyze the composition, morphology and photoelectrochemical behaviors of as-prepared samples. The possible photocatalytic mechanism for the $NiS/Cd_{0.5}Zn_{0.5}S$ nanocomposites was also discussed in detail. The hydrogen production performance of the best photocatalyst provides an important reference for the industrialization of photocatalytic hydrogen production.

2. Experimental

2.1. Materials

Cadmium acetate ($Cd(CH_3COO)_2·2H_2O$), zinc acetate ($Zn(CH_3COOH)_2·2H_2O$), thioacetamide (CH_3CSNH_2), nickel nitrate hydrate ($Ni(NO_3)_2·6H_2O$), thiourea (CH_4N_2S) were purchased from Aladdin's Reagent Company. Ethanol (C_2H_5OH), glycol ($(CH_2OH)_2$) and ethylenediamine ($NH_2CH_2CH_2NH_2$) were purchased from Sinopod Chemical Reagent Co., LTD., and lab-made deionized water was used throughout the experiment. All reagents are analytical grade with no further purification for use.

2.2. Synthesis of photocatalysts

$Cd_{0.5}Zn_{0.5}S$ sample was prepared by solvothermal method. The typical method was as follows: 5 mmol $Zn(CH_3COOH)_2·2H_2O$ and 5.00 mmol $Cd(CH_3COO)_2·2H_2O$ were firstly added to 60 mL ethylenediamine (EDA), and then 40 mmol thioacetamide was added. The mixture was continuously stirred for 1 h to be fully dissolved. The resulting mixture was transferred to 100 mL stainless steel reactor lined with polytetrafluoroethylene and reacted at 180℃ for 24 h. Next, the mixture was cooled naturally to room temperature, centrifuged and washed with ethanol and deionized water for several times, and dried overnight under vacuum at 60℃ to obtain the product. The preparation procedure of other $Cd_xZn_{1-x}S$ samples is the same as that of $Cd_{0.5}Zn_{0.5}S$, except that the molar ratio of Cd/Zn is different.

Preparation of $NiS/Cd_{0.5}Zn_{0.5}S$ nanocomposite. A certain amount of thiourea (CH_4N_2S) and nickel nitrate hydrate ($Ni(NO_3)_2·6H_2O$) were added to 72 ml glycol solution (molar ratio of 2), ultrasonic for 10 minutes, magnetic stirring for 20 minutes. Then 10 mmol $Cd_{0.5}Zn_{0.5}S$ was dispersed in the mixture and stirred for another 60 minutes. The mixture was then transferred to 100 mL Teflon-lined hydrothermal autoclave and heated at 180 ℃ for 12 h. After cooling to room temperature, the product is washed several times with deionized water and ethanol, and then dried overnight in a vacuum oven at 60 ° C. The theoretical ratios of NiS and $Cd_{0.5}Zn_{0.5}S$ in the samples was 0.15 and the synthesized samples were labeled as $NiS/Cd_{0.5}Zn_{0.5}S$.

2.3. Characterization

The crystal structure of the sample was characterized by X-ray diffractometer (XRD-7000). Field emission scanning electron microscope (SEM, Hitachi S-4800) and high-resolution transmission electron microscope (HRTEM, Talos F200X) were used to observe the morphology and microstructure of the samples. The surface composition and chemical state of the samples were determined by X-ray photoelectron spectrometer (XPS, Thermo Fisher Scientific ESCALAB 250Xi). The UV-vis diffuse reflectance spectrum is obtained on the UV-vis near infrared spectrometer (UV-vis DRS, Cary 5000). The lifetime of the sample was analyzed by Time-resolved photoluminescence spectra (TRPL, Edinburgh FLS 980).

2.4. Photoelectrochemical measurements

The three-electrode system was constructed by using the FTO glass coated with the sample as the working electrode, the Ag/AgCl standard electrode as the reference electrode, and the platinum electrode as the counter electrode. The electrolyte was 0.10 M Na_2SO_4 solution, and the photoelectrochemical properties of the samples were evaluated at the electrochemical workstation (CHI-660E, Shanghai Chenhua).

2.5. The evaluation of photocatalytic hydrogen production

The 30 mg photocatalyst was ultrasonically dispersed into the sealed reactor with 70 ml aqueous solution using lactic acid (3 vol%) as the sacrificial agent, and the oxygen in the reactor was removed by purge with nitrogen air pump for 40 min. A 300 W Xenon lamp ($\lambda \geq 400$ nm) is placed on the top of the photoreactor, and the light source is turned on to start the photocatalytic reaction. Throughout the reaction, cooling water is passed through the reactor jacket to maintain a constant reaction temperature (15 °C). The reaction was lasted for 3 h and the generated H_2 was determined by gas chromatography (GC-7920).

3. Results and discussion

3.1. Structure and performance optimization of $Cd_xZn_{1-x}S$

Using EDA as solvent, a series of $Cd_xZn_{1-x}S$ samples (x = 1.0, 0.9, 0.7, 0.5, 0.3, 0.1, 0) were prepared by solvothermal method. The XRD patterns of the samples are shown in Fig. 1. The XRD pattern shows that pure CdS is hexagonal wurtzite phase (JCPDS card No. 77-2306). When the x value is decreased to 0.7 ~ 0.3, the diffraction intensity becomes weaker. Due to the small ionic radius, Zn^{2+} (0.74 Å) can bind to the lattice of CdS or enter the gap of CdS. Compared with pure CdS, the lower crystallinity of $Cd_xZn_{1-x}S$ samples can be attributed to the crystal structure disorder or distortion caused by the inclusion of Zn^{2+} ions into CdS lattice [7,8]. Due to the formation of $Cd_xZn_{1-x}S$, (100) and (002) plane peaks appear, and a continuous shift towards higher diffraction angles is observed. However, the peak at position (101) looks more complex. In the sample with x = 0.7, higher angles are observed compared to CdS. As x is decreased to 0.5 and 0.3, the peak becomes weaker and wider. However, when x is 0.1, the peak becomes stronger and the position shifts back to a lower angle. According to the trend observed at x values of 0.7, 0.5, and 0.3, cubic phase ZnS (JCPDS card No. 05-0566) begin to form in the sample at x values of 0.3. In the sample with x ≤0.3, $Cd_xZn_{1-x}S$ and ZnS was formed. In the sample x = 0.1, cubic ZnS becomes the dominant phase. When x = 0, the $ZnS{\cdot}(EDA)_{0.5}$ complex is obtained due to the strong coordination ability of EDA to Zn^{2+} ions [9].

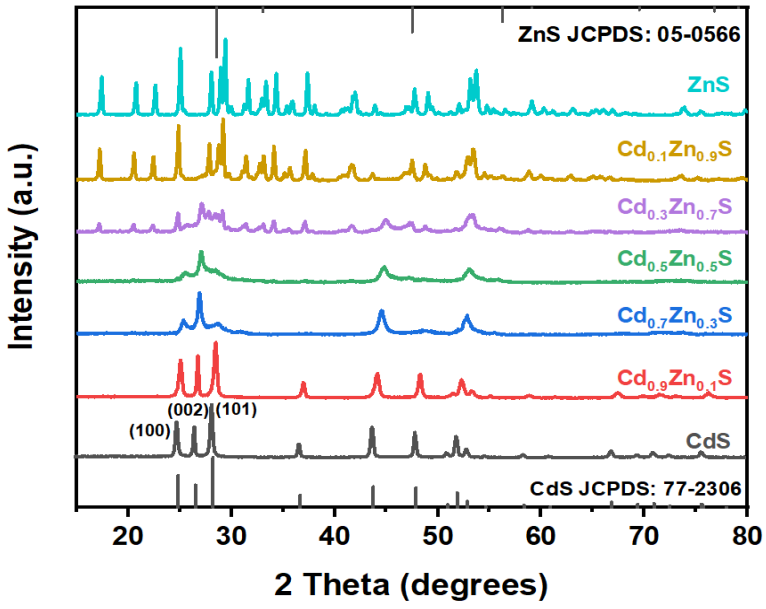

Fig. 1. XRD patterns of $Cd_xZn_{1-x}S$ (x =1.0, 0.9, 0.7, 0.5, 0.3, 0.1 and 0).

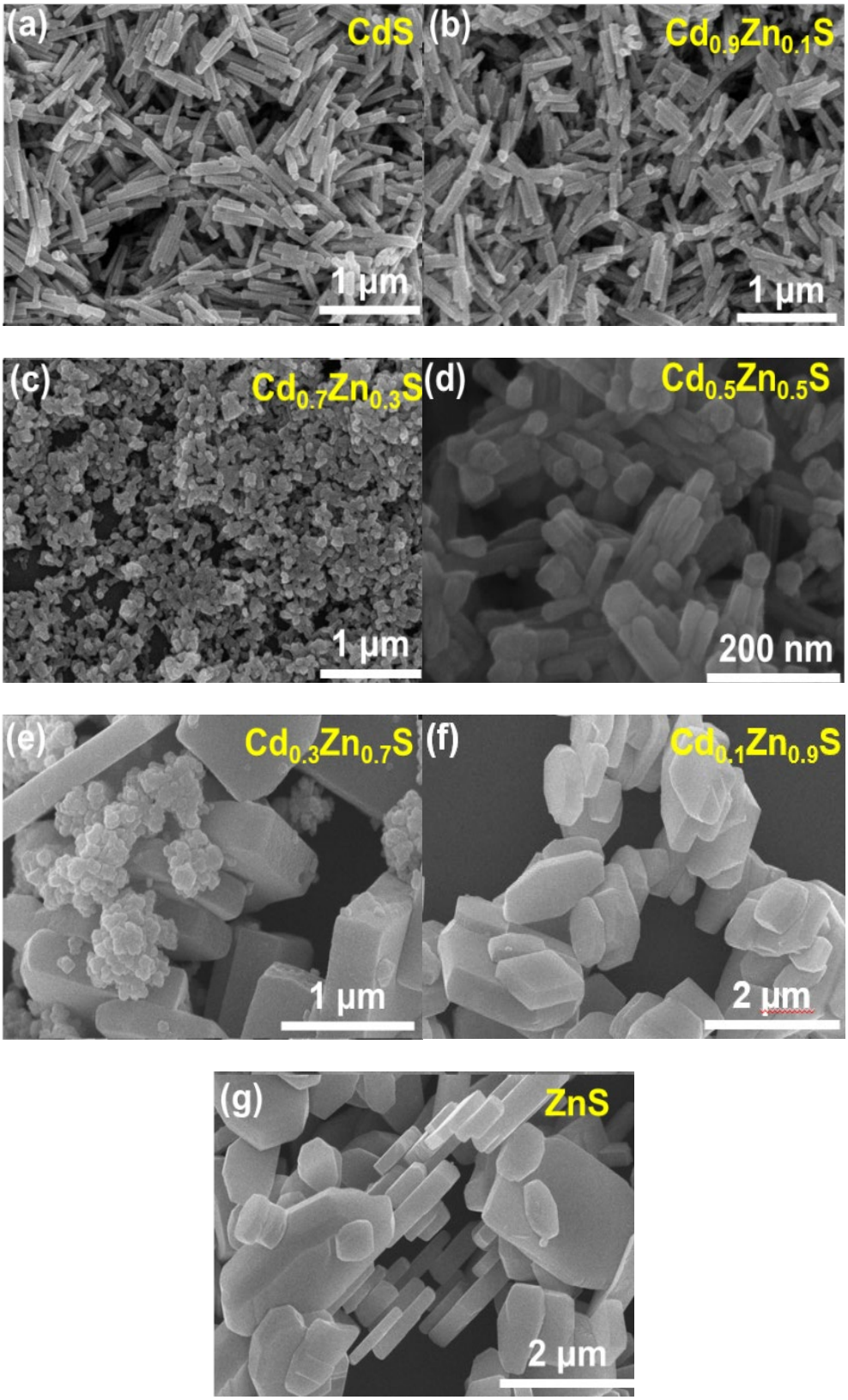

Fig. 2. SEM images of as-prepared $Cd_xZn_{1-x}S$ with x values as follows: (a) 1.0; (b) 0.9; (c) 0.7; (d) 0.5; (e) 0.3; (f) 0.1; (g) 0.

Fig. 2 shows the SEM images of prepared $Cd_xZn_{1-x}S$ samples. Because EDA facilitates CdS growth along the c-axis, pure CdS exhibit nanorods with an average length of 300 nm and a diameter of 90 nm (Fig. 2(a)). After the incorporation of Zn^{2+} ions, EDA also promoted the growth of ZnS in the x-y plane, thus delaying the preferential growth of ZnS along the c-axis direction. As a result, with the increase of Zn^{2+} content, the length of the nanorods became shorter, and the morphology of the nanorods was more like plates than nanorods. When the content of Zn^{2+} in the precursor solution was further increased to 0.7 and 0.9, CdZnS aggregates consisting of small particles and nanoplates were obtained (Fig. 2(e) and 2(f)). Finally, in the absence of Cd^{2+} ions, the $ZnS{\cdot}(EDA)_{0.5}$ complex was formed and showed plate-like shape as shown in Fig. 2(g).

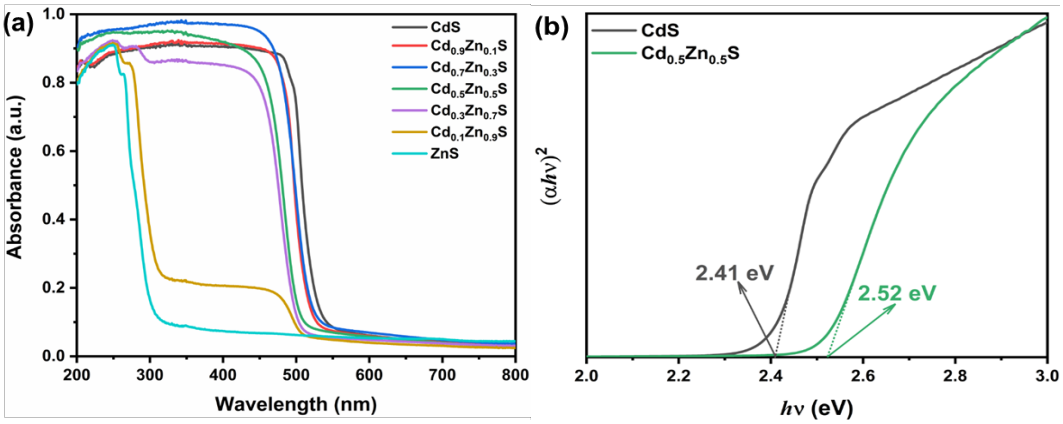

Fig. 3. (a) UV-vis DRS spectra of the samples; (b) Tauc plots of the samples.

As shown in Fig. 3(a), the absorption edges of ZnS and CdS are approximately 370 nm and 525 nm, respectively. When the content of Zn^{2+} is increased gradually in $Cd_xZn_{1-x}S$, its absorption edge has blue shift, which is caused by the incorporation of Zn^{2+} into Cd^{2+}. In addition, with the increase of Zn^{2+} content, the band gap of $Cd_xZn_{1-x}S$ is increased, which means that the band gap can be precisely adjusted by changing the composition of $Cd_xZn_{1-x}S$ [10]. As shown in Fig. 3(b), the band gap of CdS and $Cd_{0.5}Zn_{0.5}S$ are 2.41 and 2.52 eV, respectively.

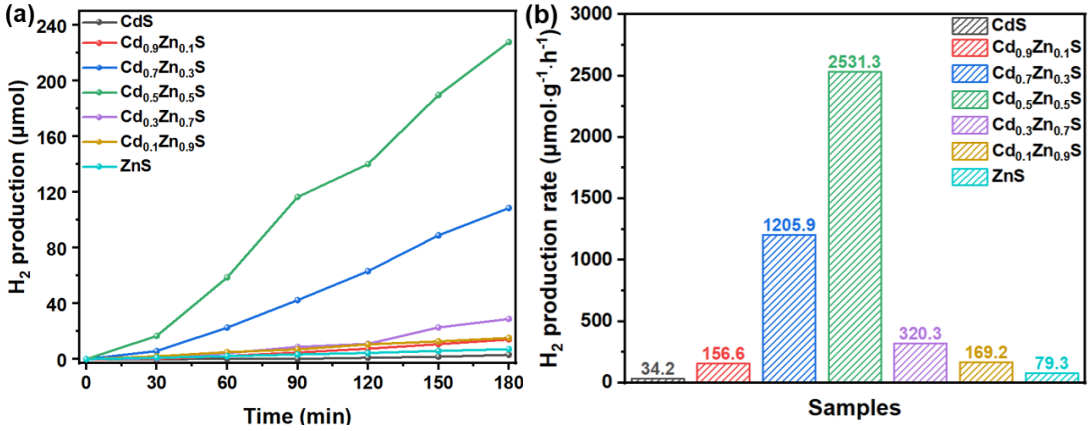

Fig. 4. Photocatalytic hydrogen production (a) and hydrogen production rate (b) of different samples under visible light irradiation with lactic acid as sacrificial agent.

Under the irradiation of visible light (λ≥400 nm), the photocatalytic hydrogen evolution properties of different samples were studied with lactic acid as a sacrificial reagent with shown in Fig. 4. The photocatalytic hydrogen production activity of $Cd_xZn_{1-x}S$ (x = 0.9, 0.7, 0.5, 0.3, 0.1)

was higher than that of pure CdS and ZnS. Pure CdS and ZnS showed relatively low photocatalytic activity during the reaction, with hydrogen production rates of 34.2 and 79.3 $\mu mol \cdot g^{-1} \cdot h^{-1}$, respectively, which was caused by the rapid recombination of photogenerated carriers in CdS and ZnS. The hydrogen production rate of the optimized $Cd_{0.5}Zn_{0.5}S$ reached 2531.3 $\mu mol \cdot g^{-1} \cdot h^{-1}$. With the increase of the molar ratio of Zn^{2+}, the photocatalytic hydrogen production rate of $Cd_xZn_{1-x}S$ samples ($x > 0.5$) is increased, which is due to the low conduction band (CB) position and small overpotential [11]. On the other hand, the photocatalytic hydrogen production rate began to decline for $Cd_xZn_{1-x}S$ ($x < 0.3$), which was caused by reduced visible light absorption and a wider band gap, which was confirmed by the results of UV-vis DRS.

Based on the above studies, the $Cd_{0.5}Zn_{0.5}S$ with the best hydrogen production performance was selected as the further research object, and the hydrogen production performance of $Cd_{0.5}Zn_{0.5}S$ was further improved with NiS loading on its surface by solvothermal method.

3.2. Structure and performance of NiS/$Cd_{0.5}Zn_{0.5}S$ nanocomposite

Fig. 5 shows TEM images of $Cd_{0.5}Zn_{0.5}S$, NiS, and NiS/$Cd_{0.5}Zn_{0.5}S$. Figs. 5(a) and 5(b) show that the diameter of pure $Cd_{0.5}Zn_{0.5}S$ nanorod is about 20 nm, and the lattice stripe with spacing of 0.34 nm (Fig. 5(b)) is ascribed to the (002) crystal face of hexagonal $Cd_{0.5}Zn_{0.5}S$ [12]. Fig. 5(c) show that NiS is an irregular overlap of layered structures. In Fig. 5(d), the lattice fringe with planar spacing of 0.29 nm corresponds to the (101) crystal faces of NiS [13]. Fig. 5(e) shows the TEM image of NiS/$Cd_{0.5}Zn_{0.5}S$ nanocomposite. After loading NiS, the morphology of $Cd_{0.5}Zn_{0.5}S$ did not change significantly, and its diameter is increased to about 30 nm. As shown in Fig. 5(f), the lattice fringes of 0.34 nm and 0.27 nm is belonged to the (002) and (300) crystal faces of $Cd_{0.5}Zn_{0.5}S$ and NiS, respectively. These results not only demonstrate the successful synthesis of NiS/$Cd_{0.5}Zn_{0.5}S$ nanocomposites, but also confirm the close contact between NiS and $Cd_{0.5}Zn_{0.5}S$, which is conducive to electron transfer.

XPS was used to study the surface composition and chemical state of the prepared photocatalyst, and the results were shown in Figure 6. As shown in Fig. 6(a), the XPS spectra of Cd 3d of sample $Cd_{0.5}Zn_{0.5}S$ show two characteristic peaks with binding energies of 404.5 eV and 411.5 eV, belonging to Cd $3d_{5/2}$ and Cd $3d_{3/2}$, respectively, indicating that Cd element appears in the form of Cd^{2+} [14]. In the Zn 2p spectrum (Fig. 6(b)), the two peaks of 1021.4 eV (Zn $2p_{3/2}$) and 1044.5 eV (Zn $2p_{1/2}$) belong to the Zn (+2) chemical state of $Cd_{0.5}Zn_{0.5}S$. In addition, the XPS spectrum of $Cd_{0.5}Zn_{0.5}S$ in Fig. 6(c) also showed two peaks, located at 161.1 eV and 162.2 eV, indicating the existence of S^{2-} [15]. Compared with pure NiS/$Cd_{0.5}Zn_{0.5}S$, the peak of S 2p in NiS/$Cd_{0.5}Zn_{0.5}S$ is transferred to a lower binding energy because the loading NiS promotes electron transfer from $Cd_{0.5}Zn_{0.5}S$ to NiS at the two-phase interface. The Ni 2p spectra of NiS/$Cd_{0.5}Zn_{0.5}S$ are shown in Fig. 6(d) and fitted into six peaks. The binding energies at 863.4 eV and 880.9 eV belong to the satellite peaks of Ni 2p, and those at 860.8 eV and 878.7 eV belong to Ni $2p_{3/2}$ and $2p_{1/2}$, indicating the presence of Ni^{2+}. The other two peaks at 855.2 eV and 872.8 eV belong to Ni $2p_{3/2}$ and Ni $2p_{1/2}$, respectively, indicating the presence of Ni^{3+}. The above results demonstrated the formation of NiS/$Cd_{0.5}Zn_{0.5}S$ heterojunction.

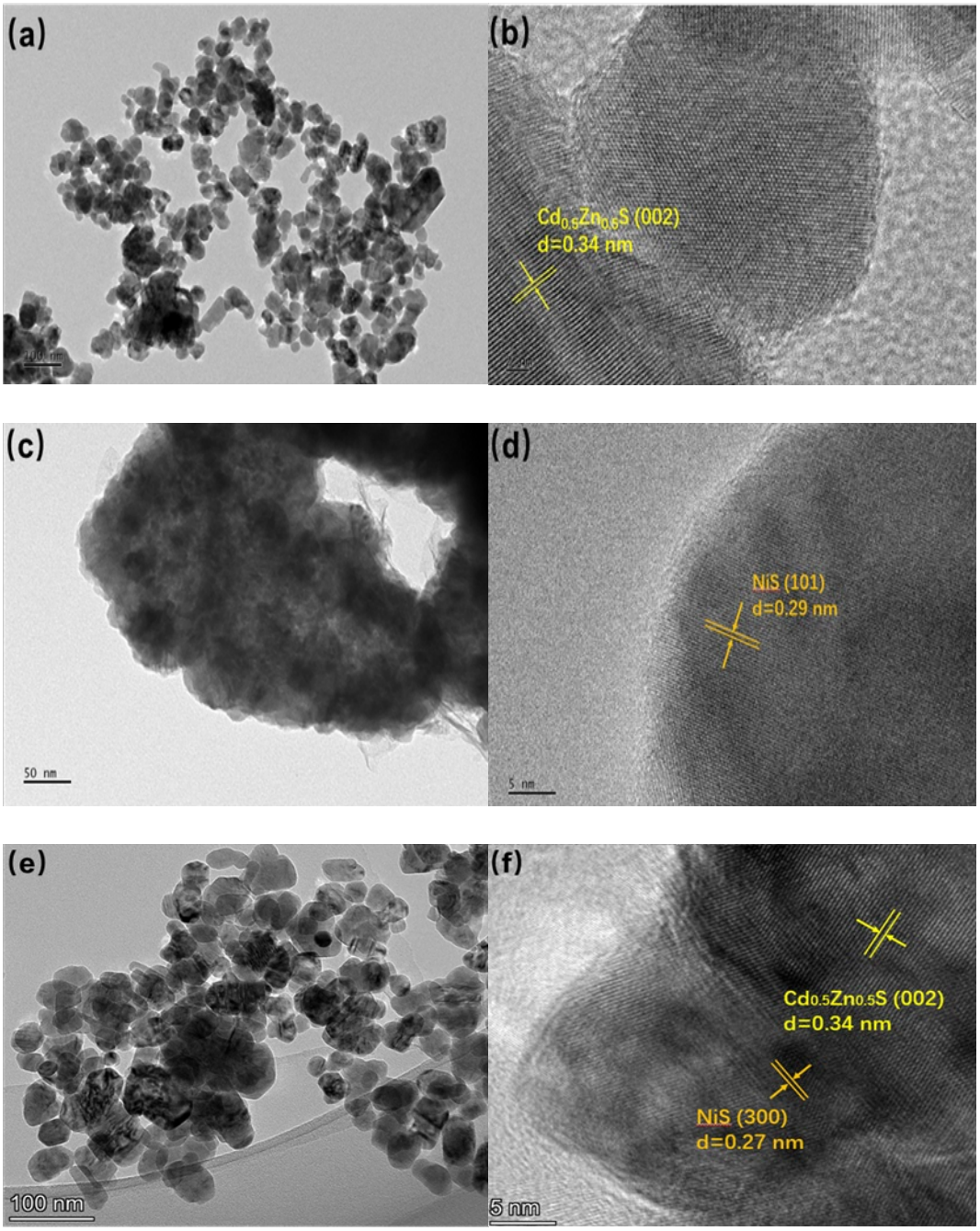

Fig. 5. TEM images of different samples: (a-b) $Cd_{0.5}Zn_{0.5}S$; (c-d) NiS; (e-f) NiS/$Cd_{0.5}Zn_{0.5}S$.

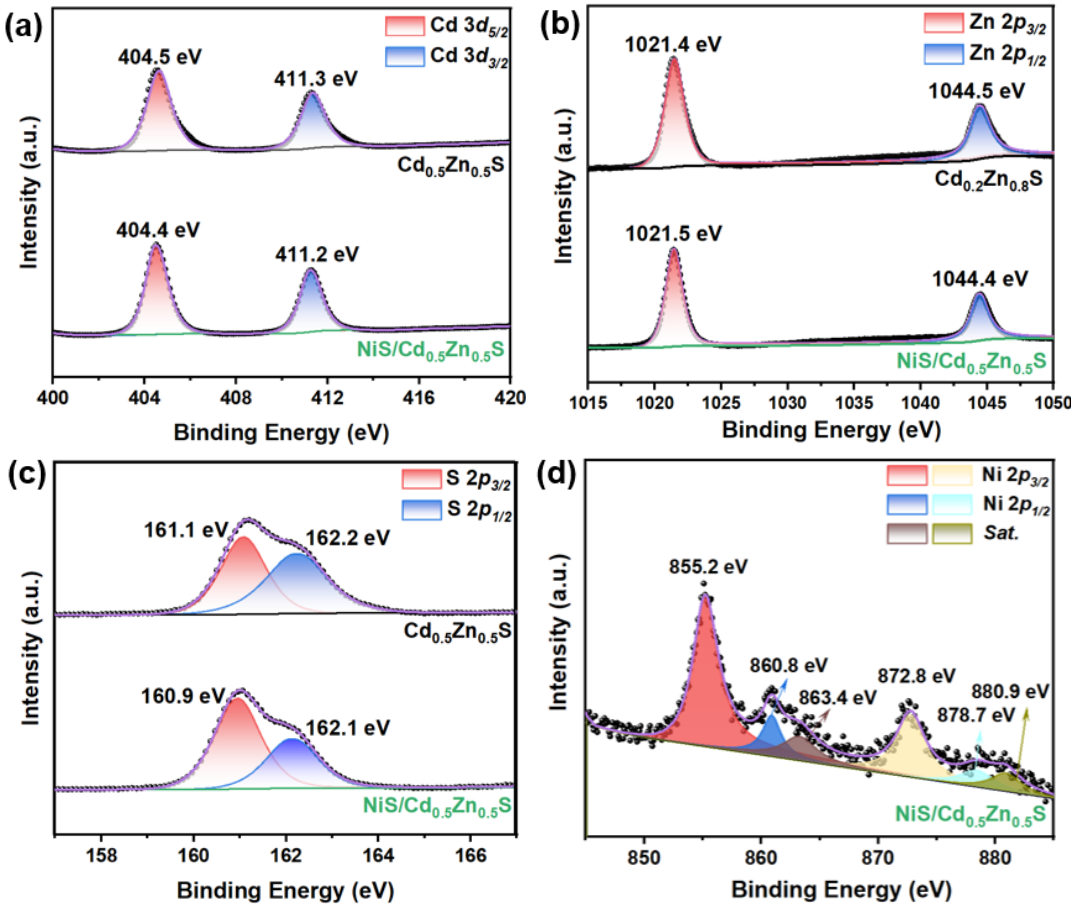

Fig. 6. XPS spectra of pure $Cd_{0.5}Zn_{0.5}S$ and $NiS/Cd_{0.5}Zn_{0.5}S$ nanocomposite: (a) Cd 3d; (b) Zn 2p; (c) S 2p; (d) Ni 2p.

The photocatalytic hydrogen evolution properties of $NiS/Cd_{0.5}Zn_{0.5}S$ nanocomposites were studied with lactic acid as a sacrificial agent under visible light. In Figure 7a, the hydrogen production reaches 409.28 μmol, and the photocatalytic hydrogen evolution rate is 4547.5 $\mu mol \cdot g^{-1} \cdot h^{-1}$, which is 1.80 times that of pure $Cd_{0.5}Zn_{0.5}S$.

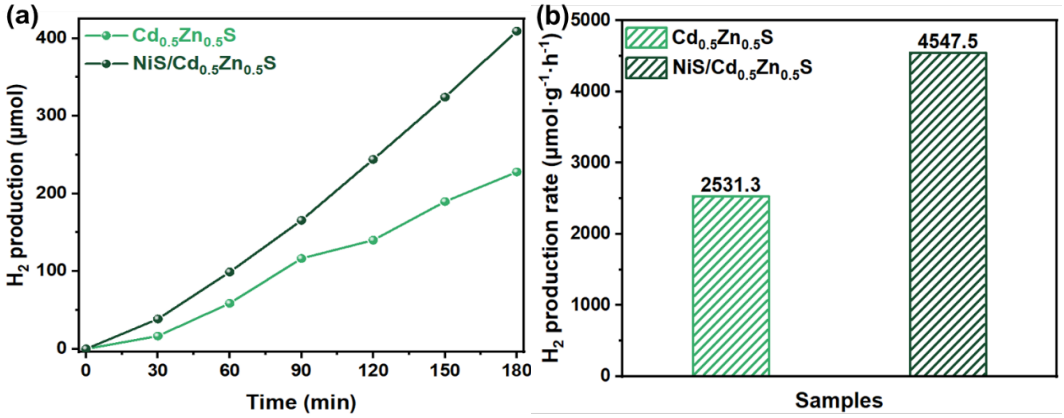

Fig. 7. Photocatalytic hydrogen production (a) and hydrogen production rate (b) of $NiS/Cd_{0.5}Zn_{0.5}S$ under visible light irradiation with lactic acid as sacrificial agent.

The charge carrier properties are studied using transient photocurrent response (Fig. 8(a)) and electrochemical impedance spectroscopy (EIS, Fig. 8(b)). Fig. 8(a) makes comparison of the photocurrent response of $Cd_{0.5}Zn_{0.5}S$ and $NiS/Cd_{0.5}Zn_{0.5}S$. $NiS/Cd_{0.5}Zn_{0.5}S$ sample shows the higher photocurrent density than that of $Cd_{0.5}Zn_{0.5}S$, indicating the superior charge separation efficiency than $Cd_{0.5}Zn_{0.5}S$. Furthermore, the same results in Fig. 8(b) are obtained by the electrochemical impedance spectroscopy (EIS). The $NiS/Cd_{0.5}Zn_{0.5}S$ exhibited a smaller radius than that of $Cd_{0.5}Zn_{0.5}S$, demonstrating the decrease of the charge transfer resistance, thus facilitating more effective charge separation and transport. The impedance curves of pure NiS (Fig. 8(b) inset) are similar in both visible and dark conditions, indicating that pure NiS exhibits only its cocatalytic properties and is not sensitive to light.

Fig. 8c shows the time-resolved photoluminescence decay profiles of $Cd_{0.5}Zn_{0.5}S$ and $NiS/Cd_{0.5}Zn_{0.5}S$. The loading of NiS in $NiS/Cd_{0.5}Zn_{0.5}S$ leads to a lower probability of the recombination of photogenerated electron and hole pairs as suggested by the increase of the photoluminescence lifetime from 2.7834 ns for $Cd_{0.5}Zn_{0.5}S$ to 3.4109 ns for $NiS/Cd_{0.5}Zn_{0.5}S$ (Fig. 8(c)) [16,17]. Fig. 8(d) shows the Mott-Schottky curve of $Cd_{0.5}Zn_{0.5}S$ with a positive slope, indicating that $Cd_{0.5}Zn_{0.5}S$ is an n-type semiconductor. The flat-band potential (E_{FB}) of $Cd_{0.5}Zn_{0.5}S$ can be obtained from the tangent line on the horizontal axis and is about -0.40 eV at pH 7 (υs. NHE). For most n-type semiconductors, E_{FB} is usually located at 0.1 eV below the CB base, so according to this feature, the CB value of pure $Cd_{0.5}Zn_{0.5}S$ can be calculated as -0.30 eV (υs. NHE). Then, with $E_{VB} = E_{CB} + E_g$, the valence band (VB) value of about 2.22 eV (υs.NHE) can be calculated.

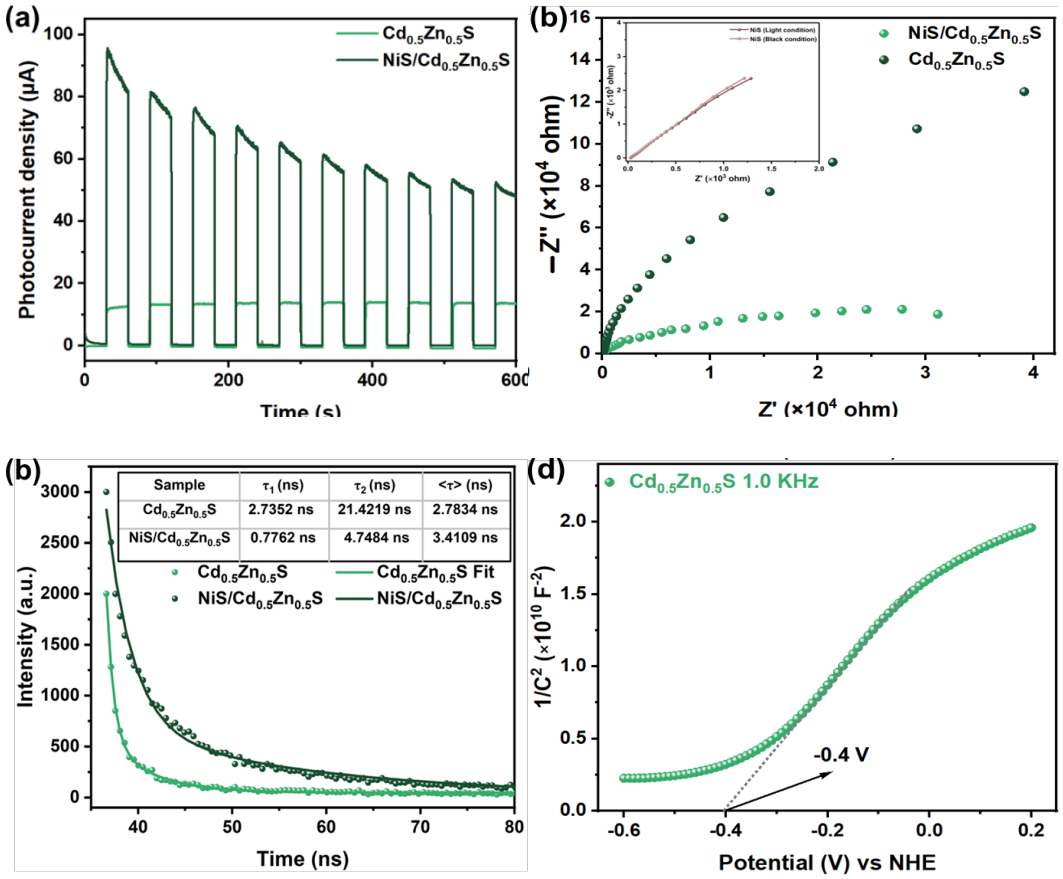

Fig. 8. (a) Transient photocurrent responses, (b) EIS Nyquist plots and (c) Time-resolved photoluminescence decay profiles of $Cd_{0.5}Zn_{0.5}S$ and $NiS/Cd_{0.5}Zn_{0.5}S$; (d) The Mott-Schottky curve of $Cd_{0.5}Zn_{0.5}S$.

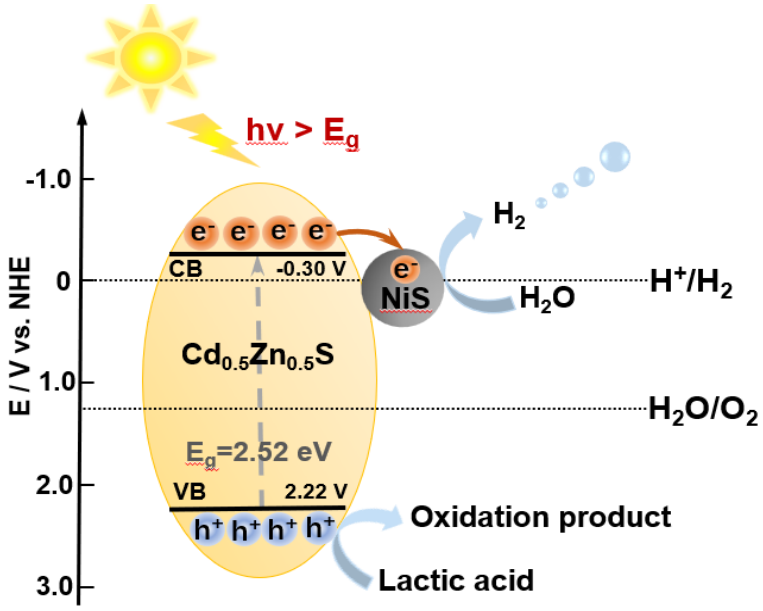

Fig. 9. Proposed photocatalytic mechanisms in NiS/$Cd_{0.5}Zn_{0.5}S$ composite photocatalyst.

According to the above analysis and experiment results, the photocatalytic mechanism of NiS/$Cd_{0.5}Zn_{0.5}S$ was proposed (Fig. 9). The $Cd_{0.5}Zn_{0.5}S$ as semiconductor can generate photoexcited electron and hole pairs under visible light irradiation, and then the electrons could transfer from VB to CB, leaving holes in the VB, then the photoexcited electrons in the CB of $Cd_{0.5}Zn_{0.5}S$ could migrated to the NiS to form an electron receiver, while the holes left in the VB of $Cd_{0.5}Zn_{0.5}S$ would react with sacrificial agent (lactic acid) to suppress the recombination of photogenerated carriers. The NiS as the cocatalyst can play the role of active sites due to its lower H_2 evolution overpotential and strong bonding tendency with H^+, which can be more easily reduced the H^+ to generate H_2 in NiS. Therefore, the addition of NiS accelerates the separation of photogenerated carriers and improves the hydrogen production activity of $Cd_{0.5}Zn_{0.5}S$.

4. Conclusion

$Cd_xZn_{1-x}S$ (x=0~1) solid solution photocatalysts with different morphologies were synthesized by solvothermal method using ethylenediamine as solvent. The light absorption of the photocatalyst was varied by changing the morphology and electronic band structure to allow strong visible light response for hydrogen generation. The results showed that the optimum $Cd_{0.5}Zn_{0.5}S$ showed a high hydrogen production rate of 2531.3 $\mu mol \cdot g^{-1} \cdot h^{-1}$. Then, the $Cd_{0.5}Zn_{0.5}S$ was loaded with NiS cocatalyst to obtain a higher photocatalytic hydrogen evolution rate of 4547.5 $\mu mol \cdot g^{-1} \cdot h^{-1}$. The hydrogen production rate of NiS/$Cd_{0.5}Zn_{0.5}S$ is 1.80 times that of pure $Cd_{0.5}Zn_{0.5}S$. The NiS could serve as a cocatalyst for the efficient capture of photogenerated electrons of $Cd_{0.5}Zn_{0.5}S$ for hydrogen generation. Our research can provide an idea for the synthesis of efficient and low cost semiconductor based photocatalysts by environmentally friendly solar hydrogen production.

Acknowledgements

This work was supported by Curriculum Ideological and Political Education Teaching Research Program of Zhejiang Province (2022), A Project Supported by Scientific Research Fund of Zhejiang Provincial Education Department (No. Y202352346), and National Innovation and Entrepreneurship Program for College Students (No. 202313291027X and No. 202310354038).

References

[1] R. Yukesh Kannah, Preethi, S. Kavitha, O. Parthiba Karthikeyan, G. Kumar, N. Vo. Dai-viet, J. Rajesh Banu, Bioresource Technology, 319, 124175 (2021); https://doi.org/10.1016/j.biortech.2020.124175

[2] P. Nikolaidis, A. Poullikkas, Renewable and sustainable energy reviews, 67, 597 (2017); https://doi.org/10.1016/j.rser.2016.09.044

[3] K. Zhang, D. Jing, C. Xing, L. Guo, International Journal of Hydrogen Energy, 32(18), 4658 (2007); https://doi.org/10.1016/j.ijhydene.2007.08.022

[4] J. Kundu, D. D. Mal, D. Pradhan, Inorganic Chemistry Frontiers, 12(8), 3055 (2021); https://doi.org/10.1039/D0QI00531B

[5] S. Jiang, L. Shen, Y. Liu, S. Qi, Z. Lu, L. Li, H. Ma, H. Wang, New Journal of Chemistry, 47, 462 (2023); https://doi.org/10.1039/D2NJ04665B

[6] W. Xue, W. Chang, X. Hu, J. Fan, E. Liu, Chinese Journal of Catalysis, 42, 152 (2021); https://doi.org/10.1016/S1872-2067(20)63593-8

[7] W. Zhao, F. Liang, Z. M. Jin, X. B. Shi, L. S. Liao, Journal of Materials Chemistry A, 2(33), 13226 (2014).

[8] Y. Wang, Z. Wang, S. Muhammad, J. He, CrystEngComm, 14(15), 5065 (2012); https://doi.org/10.1039/c2ce25517k

[9] X. Wang, L. Li, H. Gu, H. Zhang, J. Zhang, Q. Zhang, W. L. Dai, Applied Surface Science, 574, 151553 (2022); https://doi.org/10.1016/j.apsusc.2021.151553

[10] W. Dong, Y. Liu, G. Zeng, S. Zhang, T. Cai, J. Yuan, H. Chen, J. Gao, C. Liu, Journal of colloid and interface science, 518, 156 (2018); https://doi.org/10.1016/j.jcis.2018.02.018

[11] M. Liu, D. Jing, Z. Zhou, L. Guo, Nature communications, 4(1), 1 (2013); https://doi.org/10.1038/ncomms3278

[12] W. Xue, W. Chang, X. Hu, J. Fan, E. Liu, Chinese Journal of Catalysis, 42(1), 152 (2021); https://doi.org/10.1016/S1872-2067(20)63593-8

[13] H. Zhang, Z. Yu, R. Jiang, Y. Hou, J. Huang, H. Zhu, F. Yang, M. Li, F. Li, Q. Ran, Renewable Energy, 168, 1112 (2021); https://doi.org/10.1016/j.renene.2020.12.102

[14] A. P. Gaikwad, D. Tyagi, C. A. Betty, R. Sasikala, Applied Catalysis A: General, 517, 91 (2016); https://doi.org/10.1016/j.apcata.2016.03.006

[15] Q. Geng, Y. Li, H. Xie, Vacuum, 203, 111308 (2022); https://doi.org/10.1016/j.vacuum.2022.111308

[16] R. Shen, Y. Ding, S. Li, P. Zhang, Q. Xiang, Y. Hau Ng, X. Li, Chinese Journal of Catalysis, 42(1), 25 (2021); https://doi.org/10.1016/S1872-2067(20)63600-2

[17] X. Gao, D. Zeng, J. Yang, W. J. Ong, T. Fujita, X. He, J. Liu, Y. Wei, Chinese Journal of Catalysis, 42(7), 1137 (2021); https://doi.org/10.1016/S1872-2067(20)63728-7